Corrosion of Mo in KOH: Time Resolved XAFS Investigations

Dirk Lützenkirchen-Hecht* and Ronald Frahm

Institut für Materialwissenschaften und Institut für Experimentalphysik, FB 8, Bergische Universität-Gesamthochschule Wuppertal, Gaussstr. 20, D-42097 Wuppertal, Germany

Received: September 21, 2000; In Final Form: July 18, 2001

The corrosion products formed during the anodic polarization of molybdenum in 1 M KOH were investigated in situ with time-resolved X-ray absorption spectroscopy at the Mo K-edge. Near edge spectra (XANES) as well as EXAFS scans extending over approximately 1000 eV above the Mo absorption edge were measured as a function of the corrosion time. Time dependent values for the concentration of the dissolved Mo species in the electrolyte were calculated from the change of the absorption cofficient at the absorption edge. The detailed analysis of the XANES and EXAFS data suggests the presence of MoO_4^{2-} ions in the solution.

1. Introduction

Corrosion products usually appear in front of a corroded electrode in very low concentrations. They can be detected with high accuracy and time resolution using electrochemical methods such as rotating ring disk electrode (RRDE) measurements (see, e.g., refs 1,2) which are governed by thermodynamic properties, more specific by the relevant oxidation and reduction potentials. Therefore, it is not possible to determine structural information about corrosion products in the liquid phase using RRDE techniques. In the past, X-ray diffraction (XRD) has proven to give detailed structural data of liquids (e.g.[3]), especially if the anomalous scattering technique is applied, so that the contributions of different atomic pair correlation functions can be separated more easily.[4,5] However, these measurements are very time-consuming, so that they cannot be used for the structural characterization of time dependent processes such as corrosion phenomena because the concentration *c* of the corroded species varies strongly with time. In addition, *c* is usually very low compared to the concentration of the anions and cations of the basic electrolyte, whereas highly concentrated samples are essential for the application of anomalous scattering techniques (see e.g., refs 4,5). Furthermore, the corrosion products are inhomogeneously distributed in the liquid phase as a consequence of their formation at the electrode surface and their diffusion into the electrolyte, which further complicates the situation.

The extended X-ray absorption fine structure spectroscopy (EXAFS) technique is an element specific method to obtain structural information. EXAFS explores the modulations of the X-ray absorption coefficient above the absorption edge of a given element. It is caused by the scattering of the ejected photoelectrons from neighboring atoms, i.e., EXAFS cannot provide long range order structural information. However, EXAFS has furthered our basic understanding of amorphous substances, glasses and liquids owing to its ability to specify the accurate local short-range structure around the X-ray absorbing atom.[6−10] It has been shown recently, that EXAFS is well suited also for structural investigations of corrosion products.[11]

The measurement of a single EXAFS spectrum usually takes about 15−20 min in the conventional step scan mode, where the monochromator is moved from lower to higher energies in small energy steps, and all intensities are integrated for typically one second or even more. By contrast, EXAFS in the energy dispersive mode (DEXAFS) allows to record all data points of an EXAFS spectrum at the same time parallel in energy using a curved polychromator crystal and a position sensitive detector.[12,13] Thanks to the high flux insertion devices of 3rd generation storage rings, it has recently been shown that high-quality EXAFS data can be obtained even on a subsecond time scale.[14,15] Time-resolved EXAFS data can also be obtained using the Quick-scanning-EXAFS (QEXAFS) technique. In the QEXAFS mode, a conventional double crystal monochromator is slewed continuously at a high speed by means of microstepper motor drives and each data point is integrated for typically 0.01−0.2 s, so that a complete spectrum can be obtained in less than 1 min or even a couple of seconds only.[16−18] If the concentration of the investigated element is small as it is the case for the corrosion products in the solution, a very stable monochromator setup and low noise current amplifiers are necessary to record absorption data of acceptable quality in a reasonable time. In the present study, QEXAFS was used for the investigation of the corrosion products formed during the anodic polarization of Mo in alkaline KOH solution.

2. Experimental Details

The working electrode was a 0.5 mm thick Mo foil (Aldrich Chemicals, 99.99% purity) which was glued to the Teflon body of an electrochemical cell.[19] The cell was sealed by two thin Kapton foils which served as X-ray windows. A gold wire was utilized as counter electrode and a Hg/HgO/1 M KOH electrode (+0.14 V vs standard hydrogen electrode (SHE)) was used as reference electrode. All electrochemical preparations were performed in air saturated 1 M KOH (pH 13.8). The anodic dissolution of Mo was initiated by potential steps from −1.0 V to the potentials of interest. EXAFS data were collected at the ROEMO II beamline (bending magnet station,[16]) at the DORIS III storage ring (HASYLAB, DESY, Hamburg) operating at a positron energy of 4.43 GeV with injection currents of about 150 mA. A double-crystal monochromator with two flat Si (311) crystals and an energy resolution of about 5 eV at around 20 keV was used.[20] Furthermore, in the vicinity of the absorption edge, it can be assumed to a good approximation, that the full width at half-maximum of all peaks in the derivative spectrum closely resemble the energy resolution of the instrument. We estimated a value of about 5.2 ± 0.5 eV from the 1st derivatives

* To whom correspondence should be addressed. Tel: (+49) (0) 202 − 439 -3103. Fax: (+49) (0) 202 − 439 -3101. E-mail: dirklh@uni-wuppertal.de

10.1021/jp003414n CCC: $20.00
Published on Web 09/21/2001

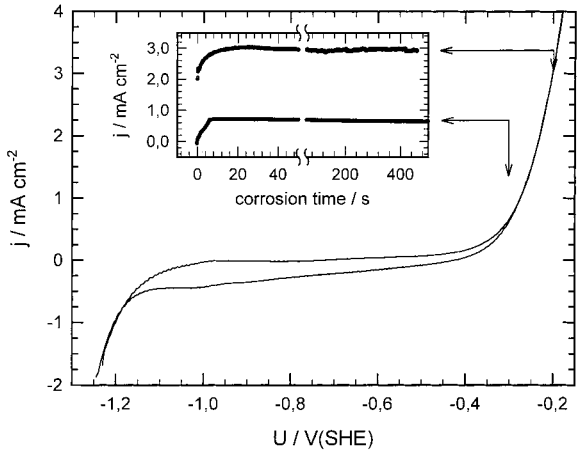

Figure 1. Potentiodynamic polarization curve (scan rate 100 mV/s) for a Mo electrode in 1 M KOH (pH 13.8). In the insert, current transients measured in situ during the polarization at −0.3 V and −0.2 V are presented, respectively.

of measured XANES spectra of a Mo-metal reference foil. The crystals were detuned with respect to each other using a piezo crystal tilt stage to reduce the amount of harmonics in the Bragg-reflected beam.[21,22] For the presented measurements, the monochromator was detuned to typically 30% of the maximum of the rocking curve. EXAFS data were collected in situ under potential control in the vicinity of the Mo K-edge at 20 keV. For this energy range, the photon flux amounts to about 10^8 photons/mm^2 s. For the experiments, the collimated X-ray beam (50−100 μm vertical, 10 mm horizontal size) passes the electrochemical cell parallel to the corroded metal working electrode, as schematically sketched in the insert of Figure 2b. Incident (I_1) and transmitted (I_2) intensities were measured by means of ionization chambers filled with Ar or Kr at atmospheric pressure and amplified by means of Keithley 428 current amplifiers. More details about the beamline electronics can be found in ref 16. Using integration times between ca. 0.05 s and ca. 0.2 s for each data point, the time resolution ranged from about 10 s up to 60 s for near edge scans and from 150 to 300 s for extended EXAFS scans. The energy scale of the monochromator was calibrated with a molybdenum foil measured in transmission between the second and a third ionization chamber simultaneously with each energy scan. A molybdenum foil and crystalline Mo-oxide powders (MoO_2 and MoO_3 obtained from Aldrich Chemicals) pressed in polyethylene were measured in transmission to obtain reference spectra. Homemade computer programs were used for the EXAFS data reduction and processing.

3. Results and Discussions

In Figure 1, the cyclic voltammogram of Mo in air saturated 1 M KOH is presented. The increasing current density anodic to ca. −0.35 V corresponds to the anodic dissolution of Mo metal. In the insert of Figure 1, current transients measured in situ during the polarization of the Mo electrode at −0.3 V and −0.2V are presented. As can be seen, approximately constant corrosion currents are obtained ∼20 s after the potential step. In Figure 2, the XANES regions of Mo K-edge absorption spectra recorded at different times after a potential step from −1.0 V to −0.3 V (Figure 2a) and to −0.2 V (Figure 2b) are presented, respectively. The increasing Mo absorption clearly indicates the increasing concentration of Mo in the solution in both cases. Therefore, time dependent values for the Mo concentration in the electrolyte can be determined from the edge heights of the spectra as follows. The change of the absorption coef-

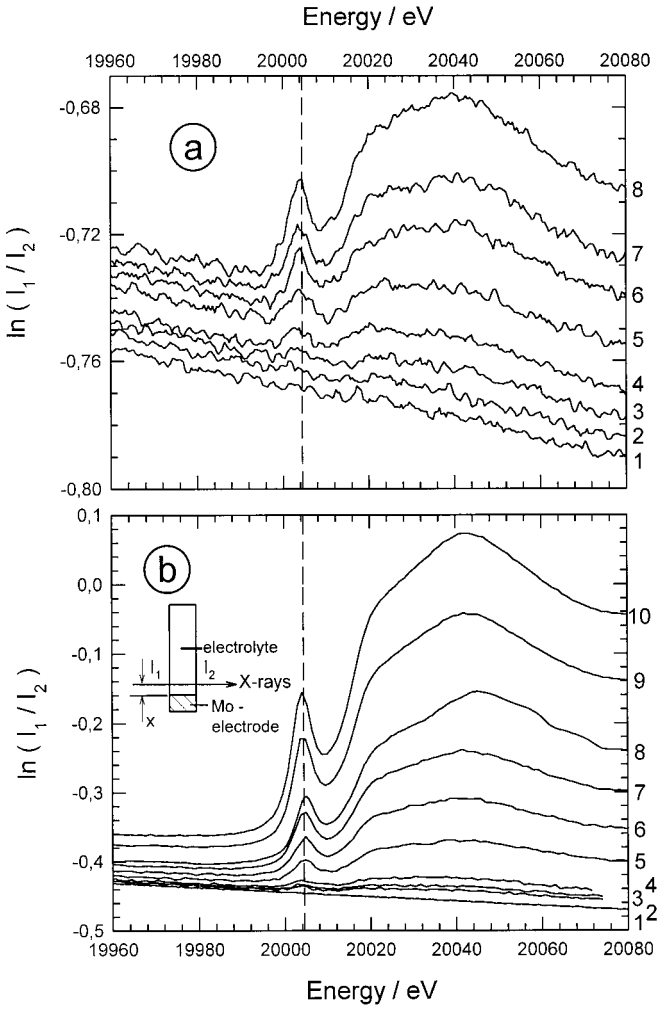

Figure 2. XANES region of Mo K-edge spectra obtained during the electrochemical corrosion of a Mo-electrode in 1 M KOH after a potential step from −1.0 V to (a) −0.3 V and to −0.2 V (b). The X-ray beam passes the electrochemical parallel to the surface of the Mo electrode in a distance x as schematically shown in the insert of Figure 2b. (a) In situ spectra 1−8 denote 0 s, 1000 s, 2000 s, 3000 s, 4030 s, 6100, 8060, and 10 040 s oxidation time, respectively with $x = 5.7$ mm. The spectra were recorded with an integration time of 0.1 s/data point resulting in a total scan time of 70 s for the photon energy range from 19 950 to 20 300 eV. (b) In situ spectra 1−10 denote 0 s, 400 s, 650 s, 920 s, 1950 s, 2500 s, 3400 s, 4300, 5300, and 6300 s of oxidation time, at $x = 3.5$ mm. Spectra 1−4 were reorded in 8.8 s (0.08 s/data point), spectra 5−10 in 12.1 s/spectrum (0.1 s/ data point).

ficient at the Mo K-absorption edge caused by a concentration c of Mo-atoms $\Delta\mu$(c) in a cell of 20 mm length can be calculated from the tabulated total mass attenuation cross sections below and above the Mo K-edge (i.e., 13.3 cm^2/g and 83.0 cm^2/g as given in refs 23,24), the mass density (10.22 g/cm^3) and the atomic concentration (6.42×10^{22} atoms/cm^3) of Mo-metal, resulting in a value of approximately $\Delta\mu(c) \approx c \times 13.36$ l/mol; i.e., a 1 millimolar Mo solution would lead to an edge height of about $\Delta\mu(c) \approx 0.013$. For the determination of the edge height in the experimental absorption spectra, a linear regression was performed in the preedge region, i.e., in the photon energy range from 19 800 to 19 990 eV. This regression was extrapolated into the energy region above the edge and subtracted from the raw data. Subsequently, the positions of the first local absorption maximum and minimum above the edge were determined from the background-corrected data and mean values of the absorption coefficient were computed for each near edge spectrum. This calculation is based on the assumption that the true Mo-

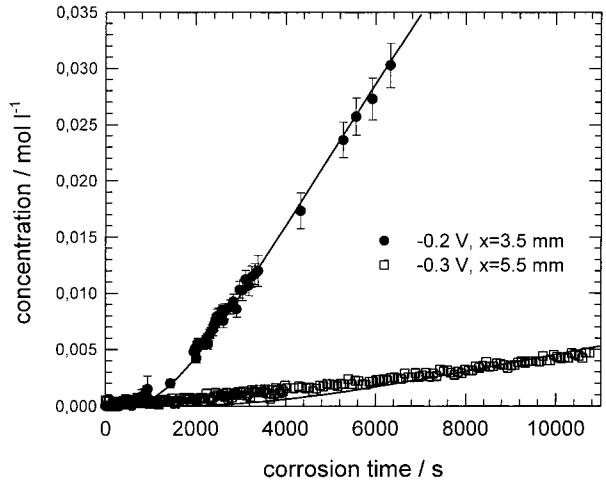

Figure 3. Concentration of Mo in the solution as calculated from the edge height of the XANES spectra in Figure 2 (dots) as a function of the corrosion time and the fit to theory (lines, see text for more details).

absorption (atomic background, see e.g., refs 25,26) is located close to the averaged absorption measured close to the absorption edge. Using these values, the concentrations shown in Figure 3 were calculated for two corrosion potentials. The error bars given for one of the experiments were computed under the assumption that the atomic background absorption may deviate up to 25% from the averaged absorption calculated from the experimental data. Because of the fact that these deviations are typically only some few percents (see refs 25,26), the given errors should be considered as an upper estimate.

The detailed analysis of the time dependence provides information about the diffusion coefficient D of the electrochemically dissolved species as follows. Under the assumption that the corrosion current (j) is constant with time (see insert of Figure 1) and using reasonable boundary conditions for the concentration of the corrosion product $c(x,t)$ (x: distance from the surface of the corroded metal electrode, t: corrosion time), Fick's equation of diffusion can be solved analytically.[27] With $c(x,t) = 0$ for $t = 0$ and $c(x,t) = 0$ for $x \rightarrow \infty$, a straightforward calculation gives

$$c(x,t) = \frac{j}{zFD}\left[2\sqrt{\frac{Dt}{\pi}}\exp\left(\frac{-x^2}{4Dt}\right) - x\left(1 - erf\left(\frac{x}{2\sqrt{Dt}}\right)\right)\right]$$

with erf (z) being the error function (see e.g., ref 27). Therefore, c(x, t) is a function of the corrosion current density j, which can be measured in situ, the valency of the corroded species z, the distance x from the surface and the diffusion coefficient D. The parameters x and j as well as $c(x, t)$ were directly measured, whereas z was determined from the XANES data (yielding $z = 6$, see below). Therefore, the diffusion coefficient D is the only independent variable, i.e., D can be determined from the measured time dependence of the concentration. The fits for both experiments are presented in Figure 3, resulting in a value $D = (1.2 \pm 0.1) \times 10^{-5}$ cm^2/s. It should be noted that similar values were found for the diffusion coefficients of Ag^+, Tl^+, Pb^{2+}, Cd^{2+}, or IO_3^- ions in aqueous solutions by using other methods.[28]

Among the determination of time dependent concentrations, the XANES spectra presented in Figure 2 provide additional electronic and structural information about the dissolved Mo-species. Besides the increase in edge intensity with time, the most conspicuous features in these spectra are the intense preedge peaks at about 20 005 eV. XANES data of molybdenum

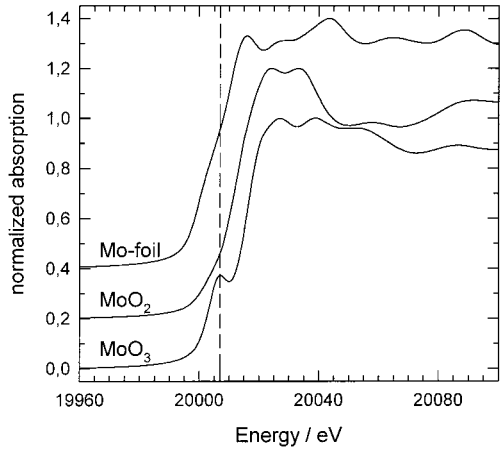

Figure 4. Mo K-edge XANES spectra of Mo reference compounds: Mo metal foil and MoO_2 and MoO_3 powders.

reference compounds MoO_2 (Mo^{4+}), MoO_3 (Mo^{6+}) and metallic Mo are depicted in Figure 4 for comparison. The edge position shifts to higher binding energy with higher oxidation state as expected. Obviously, no prepeak can be observed for MoO_2, while MoO_3 reveals a structure at around 20 007 eV. It is well-known that electronic excitations can be observed in near edge X-ray absorption spectra depending on the local geometry (see, e.g., refs 29,30). A pseudo-atomic model leads to the conclusion that the observed preedge structures may be due to 1s $\rightarrow$ 4d, 1s $\rightarrow$ 5s and 1s $\rightarrow$ 5p transitions.[31] The first of these transitions is partially allowed in a tetrahedral oxygen sphere, but it is strictly forbidden in an octahedral oxygen arrangement.[31] Therefore, the interpretation of the near edge spectra of the Mo $-$ oxides is straightforward. MoO_2 crystallizes in the rutile structure which consists of distorted Mo$-$O octahedra,[32] thus MoO_2 does not reveal a prepeak (compare ref 33). By contrast, the distorted octrahedral oxygen coordination around Mo in MoO_3 has a more complex structure with four short Mo$-$O distances between 1.67 and 1.94 Å with a structure close to a tetrahedron, and two additional long Mo$-$O distances of 2.25 and 2.33 Å, which complete a deformed octrahedral coordination;[34] thus, the existence of a preedge absorption maximum can easily be explained for MoO_3. It is well-known that the accurate energy and intensity of such a prepeak depends strongly on the local environment of the X-ray absorbing atom. For example, in Na_2MoO_4, Ba_3TiMoO_4, and $PbMoO_4$, which are all composed of nearly ideal MoO_4 tetraeders, the prepeak is more intense and shifted toward a lower photon energy of about 20 005 eV compared to MoO_3, while ammonium heptamolybdate $(NH_4)_6Mo_7O_{24} \times 4\ H_2O$, which reveals a distorted octahedral symmetry similar to MoO_3, reflects the spectral features of MoO_3 with a lowered intensity and a higher energy of the prepeak.[33] In summary, from the analysis of the Mo preedge data and the position of the absorption edge, one can easily conclude that the Mo corrosion product in KOH is a Mo^{6+} species, very likely in a tetrahedral bond geometry. This is further supported by XANES spectra calculated with the ab initio multiple-scattering code FEFF 8.0.[35] Assuming a tetrahedral bond geometry and a Mo$-$O distance of 1.76 Å (see below), the prepeak at about 20 005 eV as well as the energy depencence of the absorption coefficient above the edge can be well reproduced.[36] In addition, calculated XANES spectra and experimental data of isolated MoO_4^{2-} complexes[30] reveal edge positions and prepeak intensities very similar to those observed for the corrosion products.

In Figure 5, extended energy scans covering more than 1000 eV postedge data are presented for 5300, 5600, and 6300 s

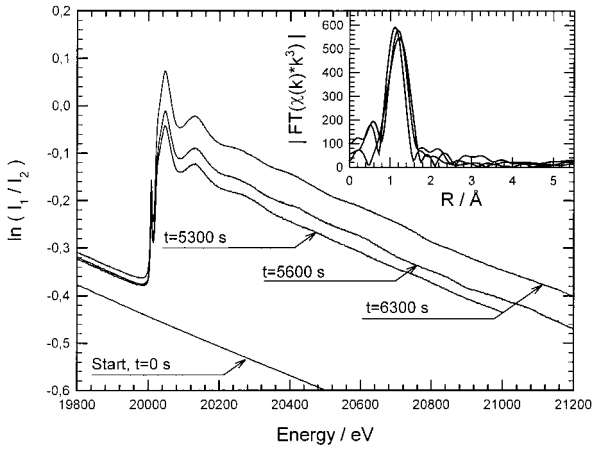

Figure 5. Transmission EXAFS-spectra recorded in situ in an electrochemical cell after 5300 s (0.15 s/data point, 150 s/spectrum), 5600 and 6300 s (0.2 s/data point, 230 s/spectrum) of oxidation at −0.2 V. For comparison, the spectrum recorded at −1.0 V previous to the oxidation is also presented. In the insert, the magnitude of the Fourier transform of the k^3-weighted fine structure oscillations $\chi(k)*k^3$ is shown (k range: 2 Å^{-1} ≤ k ≤ 10 Å^{-1}, the data are not phase shift corrected).

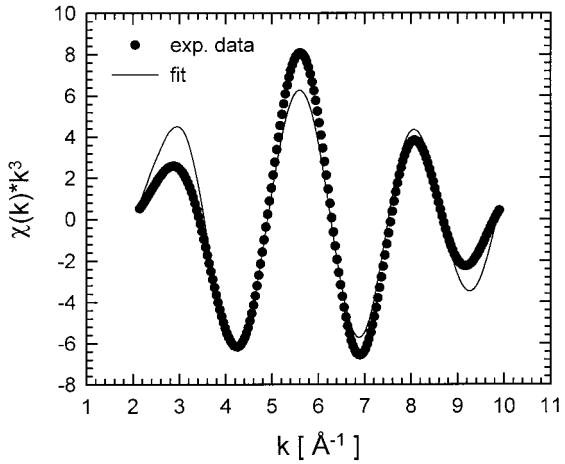

Figure 6. Typical fit of back-transformed nearest neighbor EXAFS-data $\chi(k)*k^3$ (−0.2 V, t = 5300 s) with a Mo−O coordination. The fit results obtained from this data set are R_1 = 1.75 Å, N_1 = 3.97, σ_1 = 0.067 Å and ΔE_{01} = −2.0 eV, Values for reduced $(\Delta\chi)^2$ and the fit residual $\mathscr{R}$ are $(\Delta\chi)^2$ = 5.5 and $\mathscr{R}$ ≈ 2.7%, respectively.

corrosion time. For comparison, the spectrum recorded at −1.0 V is also shown. The mean signal-to-noise ratio (S/N) of these spectra is about 100. Again, the increase in concentration with time can be easily seen. Fine structure oscillations are visible above the Mo K-edge in the whole data range presented. After conversion to the photoelectron wavenumber scale, the origin of which is given by the first inflection point of the absorption spectrum, the absorption fine structure data

$$\chi(k) = (\mu(k) - \mu_0(k))/\mu_0(k)$$

were calculated after the subtraction of a nonoscillating background $\mu_0(k)$ using common procedures which are described in the literature (see e.g., ref 6). We used cubic spline functions for the calculation of $\mu_0(k)$. The number of spline knots and the stiffness of the splines were optimized in order to obtain rigid background curves at low k values, symmetric peak shapes and a minimization of low R peaks in the Fourier Transformed signals. The Fourier Transforms (FTs) were obtained using a Bessel window function and k^3-weighted experimental $\chi(k)$ data.

In the insert of Figure 5, the magnitude of the FT of the extracted fine structure data $\chi(k)*k^3$ are presented (k range for the FT: 2 Å^{-1} ≤ k ≤ 10 Å^{-1}). Peaks in these FTs can generally be associated with coordination spheres around the absorbing atom. Here, only one single coordination shell belonging to the nearest neighbor bond is visible at about 1.2 Å radial distance; i.e., there is only one single backscattering atom detectable. Owing to the phase shifts occurring during the scattering processes, the distances in the FTs are shifted toward lower distances by about 0.4 Å compared to the real crystallographic data. For the further data evaluation, the contributions to the first coordination shell between R = 0.5 Å and R = 1.8 Å were separated by means of a filter function, back-transformed into k-space using Hanning window functions and fitted with phases and amplitudes calculated with FEFF 6.01[37] in the k range from 2.2 Å^{-1} to 10.0 Å^{-1}. EXAFS data fitting and simulation was performed according to the standard EXAFS equation (see, e.g., ref 37). A typical fit of an experimental data set with a single Mo−O shell is presented in Figure 6. Keeping in mind that the concentration of Mo in the solution is very small and that the absorption data were collected in a couple of seconds only, the fit quality appear reasonable. Fit residuals $\mathscr{R}$ were calculated from the unweighted difference between the experimental and calculated $\chi(k)$ and normalized to the experimental data in k-space. Typical values amount to about $\mathscr{R}$ ≈ 2.5%, indicating that the fit is limited by systematic errors in the model calculation.[38]

In addition, we performed a detailed error analysis as described below. Taking into account the finite Fourier Transformation range in R-space (ΔR) and the limited fitting range in k-space (Δk), the total number of independent data points that can be fitted simultaneously is given by $N_{idp} \approx (2/\pi)\,\Delta k\,\Delta R$.[39] N_{idp} is a measure of the total amount of information contained in an EXAFS spectrum; i.e., N_{idp} is the maximum number of parameters that can be determined by a fit to the spectrum.[39] Using the equation above, N_{idp} was determined to about 9 for the $\chi(k)$ spectra of the corrosion products analyzed in this study. Thus, for a single shell EXAFS fit with 4 independent fit parameters (nearest neighbor distance R_1, coordination number N_1, mean square displacement σ_1 and inner potential shift ΔE_{01}) and keeping the passive electron reduction factor S_0^2 fixed to S_0^2 = 1, the remaining freedom ν is $\nu = N_{idp} - 4 \approx 5$. In a second step, a reduced $(\Delta\chi)^2$ was calculated according to[38]

$$(\Delta\chi)^2 = \frac{N_{idp}}{N\epsilon^2}\sum_{i=1}^{N} |\chi_i^{Exp} - \chi_i^{Calc}|^2$$

with N the total number of data points, ϵ the measurement uncertainty (rms error − which was calculated from the experimental $\chi(k)$-data by a Fourier-filtering technique) and χ_i^{Exp} and χ_i^{Calc} the experimental and calculated data points, respectively. With $(\Delta\chi)^2$ as defined above, a fit can be considered acceptable, if $(\Delta\chi)^2 \approx \nu$.[38] For the performed fits, the determined values for $(\Delta\chi)^2$ ranged from about 4−6. For examples, for the fit presented in Figure 6, a value $(\Delta\chi)^2$ = 5.5 was found, compared to ν = 4.4. Therefore, the near range order structural data given below are reasonable. The averaged values determined from the fits are R_1 = 1.75 ± 0.02 Å, N_1 = 4.06 ± 0.11, σ_1 = 0.061 ± 0.005 Å and ΔE_{01} = −3.1 ± 1.2 eV. For comparison, EXAFS data analysis and $\chi(k)$ fits were also carried out using WinXas V2.1.[40] The results obtained using this software package were within in the confidence limits given above. From the determined coordination number of about N = 4, the absence of further coordination shells in the Fourier Transforms of our EXAFS data and the presence of a Mo^{6+}

TABLE 1: Literature Data for the nearest Neighbor Mo−O Bond Distances for Several Molybdate Compounds

compound	Mo−O bond distance (Å)	reference
K_2MoO_4	1.76	[41, 42]
$PbMoO_4$	1.772	[43]
$\alpha MnMoO_4$	1.761	[44]
$VOMoO_4$	1.762	[45]
$ZnMoO_4$	1.764	[46]
$CuMoO_4$	1.772	[47]

species, it can be concluded that MoO_4^{2-}-ions are formed during the corrosion of Mo in alkaline media. In addition, the small Mo−O bond distance of about 1.75 Å is also very typical for molybdates, i.e., Mo in a tetrahedral arrangement with four surrounding oxygen atoms. For comparison, binding radii determined for several different molybdates are summarized in Table 1. It should also mentioned that identical bond distances and coordination numbers were found for aqueous solutions and hydrated crystalline powders of Na_2MoO_4 and K_2MoO_4,[41] so that it was concluded that this bond length of about 1.76 Å is an intrinsic property of the MoO_4^{2-} group.[44] In addition, also the bond angles determined from X-ray diffraction data are in general very close to that of a hypothetical tetraeder (see ref 44). We can therefore give strong evidence for the presence of MoO_4^{2-} ions during the electrochemical corrosion of Mo-metal in alkaline solution.

4. Conclusions

Time-resolved X-ray absorption spectroscopy (QEXAFS) was applied to the investigation of the corrosion of molybdenum in 1 M KOH. XANES data indicate the presence of a Mo^{6+} species and the appearance of a strong preedge peak suggests a tetrahedral coordination with oxygen. The latter is confirmed by a detailed analysis of the extended X-ray absorption fine structure data which gave strong evidence for the formation of MoO_4^{2-}-ions during the electrochemical dissolution of Mo in the alkaline KOH solution. The determined Mo−O bond distance is very similar to that of crystalline molybdates with a tetrahedrally arrangement of the oxygen nearest neighbors. For the first time, the diffusion coefficient of an electrochemically dissolved species was also derived from time-resolved X-ray absorption experiments. The determined values are in good agreement with values published in the literature for other ions. Therefore, it can be concluded that QEXAFS offers unique opportunities for time-resolved in situ investigations of corrosion products in the liquid phase, so that the processes at the electrode/electrolyte interface can be analyzed comprehensively. For the future, it seems to be promising to investigate the behavior of Mo in Mo-containing alloys and steels under corrosive conditions with X-ray absorption spectroscopy in order to understand e.g., the influence of Mo alloying on the corrosion resistance of steels.[48]

Acknowledgment. We acknowledge the help of A. Krämer and S. Grundmann during the beamtimes at HASYLAB. The experiments were financially supported by the Ministerium für Schule, Wissenschaft und Forschung des Landes Nordrhein-Westfalen (MSWF NW) under Project No. 515−106 037 98 and HASYLAB.

References and Notes

(1) Albery, W. J.; Hitchman, M. L. *Ring Disk Electrodes*; Clarendon Press: Oxford, 1971.

(2) Engelhardt, G.; Schaepers, D.; Strehblow, H.-H. *J. Electrochem. Soc.* **1992**, *139*, 2170.

(3) Palinkas, G.; Kalman, E. In *Diffraction Studies on Noncrystalline Substances*; Hargittai, I., Orville-Thomas, W. J., Eds.; Elsevier Science Publishers, B. V.: Amsterdam, 1981.

(4) Kortright, J.; Warburton, W.; Bienenstock, A. Anomalous X-ray scattering and ist relationship to EXAFS. In *EXAFS and Near Edge Structure*; Bianconi, A., Incoccia, L., Stipcich, S. Springer-Verlag: Berlin, Heidelberg, 1983; 362.

(5) Schultz, E.; Bertagnolli, H.; Frahm, R. *J. Chem. Phys.* **1990**, *92*, 667.

(6) Koningsberger, D. C., Prins, R., Eds. *X-ray Absorption: Principles, Applications, Techniques of EXAFS, SEXAFS and XANES*; John Wiley & Sons: New York, 1988.

(7) Sandstrom, D. R.; Lytle, F. W. *Annu. Rev. Phys. Chem.* **1979**, *30*, 215.

(8) Sandstrom, D. R.; Stults, B. R.; Greegor, R. B. Structural Evidence for Solutions from EXAFS-Measurements. In *EXAFS Spectroscopy, Techniques and Application*; Teo, B. K., Joy, D. C., Eds.; Plenum: New York, 1981; 139.

(9) Tsutsui, Y.; Sugimoto, K.; Wasada, H.; Inada, Y.; Funahashi, S. *J. Phys. Chem. A* **1997**, *101*, 2900.

(10) Licheri, G.; Pinna, G. In *EXAFS and Near Edge Structures*; Bianconi, A., Incoccia, L., Stipcich, S., Eds.; Springer-Verlag: Berlin, Heidelberg, 1983; 240.

(11) Lützenkirchen-Hecht, D.; Waligura, C. U.; Strehblow, H.-H. *Corrosion Sci.* **1998**, *40*, 1037.

(12) Matsushita, T.; Kaminaga, U. *Jpn. J. Appl. Crystallogr.* **1980**, *13*.

(13) Hagelstein, M.; Ferrero, C.; Hatje, U.; Ressler, T.; Metz, W. *J. Synchr. Rad.* **1995**, *2*, 174.

(14) Pascarelli, S.; Neisius, T.; DePanfilis, S. *J. Synchr. Rad.* **1999**, *6*, 1044.

(15) Ressler, T.; Timpe, O.; Neisius, T.; Find, J.; Mestl, G.; Dieterle, M.; Schlögl, R. *J. Catal.* **2000**, *191*, 75.

(16) Frahm, R. *Rev. Sci. Instrum.* **1989**, *60*, 2515.

(17) Frahm, R. *Physica B* **1989**, *158*, 342.

(18) Frahm, R. *Synchr. Rad. News* **1995**, *8 (5)*, 38.

(19) Borthen, P.; Strehblow, H.-H. *Hasylab Annual Report* **1993**, 883.

(20) see: http://www-hasylab.desy.de/facility/experimental_stations_neu/stations_neu/X1.htm.

(21) Batterman, B. W.; Bilderback, D. H. X-ray Monochromators and Mirrors. In *Handbook of Synchrotron Radiation*; Broen, G., Moncton, D. E., Eds.; Elsevier Science Publishers, B. V.: Amsterdam, 1991, Vol. 3.

(22) Krolzig, A.; Materlik, G.; Swars, M.; Zegenhagen, J. *Nucl. Instrum. Methods Phys. Res.* **1984**, *219*, 430.

(23) *Handbook of Spectroscopy*; J. W. Robinson, Ed.; CRC Press: Cleveland (Ohio) 1974.

(24) Henke, B. L.; Gullikson, E. M.; Davis, J. C. *Atomic Data and Nuclear Data Tables* **1993**, *54 No. 2*, (July 1993).

(25) Rehr, J. J.; Booth, C. H.; Bridges, F.; Zabinsky, Z. I. *Phys. Rev. B* **1994**, *49*, 12347.

(26) Rehr, J. J.; Zabinsky, Z. I.; Ankudinov, A.; Albers, R. C. *Physica B* **1995**, *208&209*, 23.

(27) Bockris, J. O'M.; Reddy, A. K. *Modern Electrochemistry*; Plenum Press: New York, 1977; 287, Vol. 1 .

(28) Heyrovský, J.; Kuta, J. *Principles of Polarography*; Academic Press: New York, 1966.

(29) Lengeler, B. *Adv. Mater.* **1990**, *2*, 123.

(30) Kutzler, F. W.; Natoli, C. R.; Misemer, D. K.; Doniach, S.; Hodgson, K. O. *J. Chem. Phys.* **1980**, *73*, 3274.

(31) Chiu, N. S.; Bauer, S. H.; Johnson, M. F. L. *J. Catal.* **1984**, *89*, 226.

(32) Brandt, B. G.; Stapski, A. C. *Acta Chim. Scand.* **1967**, *21*, 661.

(33) von Hippel, L. M. J.; Hilbrig, F.; Schmelz, H.; Lengeler, B.; Knözinger, H. *Collect. Czech. Chem. Commun.* **1992**, *57*, 2465.

(34) Gmelin, *Handbuch der Anorganischen Chemie, 8. Aufl., Molybdän, Ergänzungsband B2*, Springer-Verlag: Berlin, Heidelberg, New York, 1986.

(35) Ankudinov, A. L.; Ravel, B.; Rehr, J. J.; Conradson, S. D. *Phys. Rev. B.* **1998**, *58*, 7565.

(36) Lützenkirchen-Hecht, D. unpublished.

(37) Rehr, J. J.; Albers, R. C.; Zabinsky, Z. I. *Phys. Rev. Lett.* **1992**, *69*, 3397.

(38) Stern, E. A.; Newville, M.; Ravel, B.; Yacoby, Y.; Haskel, D. *Physica B* **1995**, *208 & 209*, 117.

(39) Stern, E. A. *Phys. Rev. B* **1993**, *48*, 9825.

(40) Ressler, T. *J. Synchrotron Rad.* **1998**, *5*, 118.

(41) Cramer, S. P.; Hodgson, K. O.; Stiefel, E. I.; Newton, W. E. *J. Am. Chem. Soc.* **1978**, *100*, 2748.

(42) Gatehouse, B. M.; Leverett, P. *J. Chem. Soc. A* **1969**, 849.

(43) Leciejewicz, J. *Z. Kristallogr.* **1965**, *121*, 158.

(44) Abrahams, S. C.; Reddy, J. M. *J. Chem. Phys.* **1965**, *43*, 2533.

(45) Eick, H. A.; Kihlborg, L. *Acta Chem. Scand.* **1966**, *20*, 722.

(46) Abrahams, S. C. *J. Chem. Phys.* **1967**, *46*, 2052.
(47) Abrahams, S. C.; Bernstein, J. L.; Jamieson, P. B. *J. Chem. Phys*. **1968**, *48*, 2619.
(48) Strehblow, H.-H. *Localized Corrosion and its Relation Towards the Formation of Cation Complexes with Aggressive Anions*, Joint International Meeting October 6−11: San Antonio, Texas, 1996.